Check for updates

Probiotics mitigate thermal stress- and pathogen-driven impacts on coral skeleton

Mahdi Moradi[1‡], Phillipe R. Magalhaes[2], Raquel S. Peixoto[2,3],
Cassia C.A.C. Jonck[1], Daniel François[1†], Anna Clara F. Bellot[1],
Jonatã B. Teixeira[1], Carla S. Silveira[1], Gustavo Duarte[2,3],
Heitor Evangelista[4] and Catia F. Barbosa[1*]

[1]Departamento de Geoquímica, Programa de Pós-graduação em Geoquímica, Universidade Federal
Fluminense/UFF, Niterói, Rio de Janeiro, Brazil, [2]Red Sea Research Center (RSRC), Biological and
Environmental Sciences and Engineering Division (BESE), King Abdullah University of Science and
Technology (KAUST), Thuwal, Saudi Arabia, [3]Laboratory of Molecular Microbial Ecology, Instituto de
Microbiologia Paulo de Góes, Universidade Federal do Rio de Janeiro/UFRJ, Rio de Janeiro, Brazil,
[4]Universidade do Estado do Rio de Janeiro-UERJ/LARAMG, Rio de Janeiro, Brazil

Threats leading to a reduction in coral populations are apparent worldwide. Several different approaches have been tested to accelerate the adaptation of corals to a changing climate. Here, we evaluated the skeleton structure, crystal habit, and chemical changes of the coral *Pocillopora damicornis* in response to the pathogen (*Vibrio coralliilyticus*) and probiotic (Beneficial Microorganisms for Corals, BMCs) inoculation under ambient conditions (26 °C) and thermal stress (30 °C) during a 50-day mesocosm experiment. The skeletons were analyzed using microtomography, energy-dispersive x-ray spectroscopy (EDX/SEM), and densitometry to investigate the skeleto-physico-chemical micro-morphological changes in porosity, median pore-size diameter, crystal habit, Mg/Ca, Sr/Ca, the skeleton mineral density (g/cm^2) and skeleton mineral content (g^{-2}). The results indicate considerable changes in the coral skeleton caused by both temperature and microbial inoculation. Most importantly, lower density (to ~ x̄ 0.5 g/cm^2) and higher porosity (up to ~ x̄ 47%) were correlated with inoculation of *V. coralliilyticus* and mitigated by probiotics. BMCs also substantially increased calcification, as evidenced by Mg/Ca in the skeleton of thermally stressed corals. At the micron scale, aragonite crystal fibbers precipitated during the experiments showed an acicular habit in thermally stressed and pathogen-inoculated corals kept at 30 °C. In contrast, a spherulitic habit, characteristic of high growth rates, was observed in corals inoculated with both BMCs and *V. coralliilyticus*. Our findings reveal that pathogen inoculation and thermal stress had notable impacts on coral skeleton properties, including porosity, density, and crystal morphology, in a short period of time, which highlights the potential impacts of shifts in climate warming and environmental quality. Interestingly, BMCs played a role in maintaining the properties of skeleton calcification.

KEYWORDS

Pocillopora damicornis, micro-morphologies, porosity, coral calcification, probiotics, disease, climate change, *Vibrio coralliilyticus*

1 Introduction

Elevated pCO$_2$ and sea surface temperatures, in addition to lower seawater pH caused by climate change, have sharply increased the risk of the extinction of coral reefs (Carpenter et al., 2008; Mollica et al., 2018; Knowlton et al., 2021). These factors could reduce carbonate production, generating positive feedback that amplifies the initial signs of these forcings. The production of carbonate by corals, which comprises a good part of the carbonate produced in the world's oceans and is crucial for the global carbon cycle, has been impaired by global change (Milliman, 1993; Cornwall et al., 2021; Braz et al., 2022).

The current decline of coral populations is worldwide and results directly and indirectly from human activities, ranging from misguided tourism and fishing practices to the more insidious threat posed by accelerating levels of thermal bleaching and consequently disease outbreaks (Bruno et al., 2007). It is estimated that, considering the worst-case scenario of the Intergovernmental Panel on Climate Change communications, up to 94% of coral reefs will be eroding by 2050 (Cornwall et al., 2021). Therefore, major scientific, governmental, and philanthropic entities have been discussing and developing solutions to mitigate the factors leading to coral reef declines (Knowlton et al., 2021) and aid corals in adapting to the current scenario and persisting until climate neutrality is reached (Voolstra et al., 2021). Bleaching threats leading to a reduction in coral populations are apparent around the world and only tend to grow and compromise the calcification and survival of these species of wide geographic occurrence. The increased vulnerability of corals to higher seawater temperatures has reduced their resistance to pathogens (Ward et al., 2007; Rodriguez-Lanetty et al., 2009) and their calcification rates (Howe and Marshall, 2002; Reynaud et al., 2003) and has increased the incidence of changes in the skeletal formation (Foster et al., 2016). Recent guidelines have highlighted the urgent need for a bold commitment to three specific pillars that may allow coral reefs to persist: mitigation of CO$_2$ emissions, mitigation of local impacts, and active restoration and innovation (Knowlton et al., 2021). Regarding active restoration and innovation, corals are holobionts, i.e., organisms composed of the host in close association with microorganisms and viruses. Different compartments of these holobionts have proven to be able to adapt to environmental shifts and are important targets for coral rehabilitation (Voolstra et al., 2021). For instance, the "coral probiotic hypothesis" (CPH) asserts that the coral microbiome can increase coral resistance in stressful conditions (Reshef et al., 2006). This microbiome includes some specific symbionts termed beneficial microorganisms for corals (BMCs, or coral probiotics) (Peixoto et al., 2017; Peixoto et al., 2021), which have proven to protect corals against toxic compounds (Fragoso dos Santos et al., 2015; Silva et al., 2019), mitigate coral bleaching (Rosado et al., 2019; Doering et al., 2021; Santoro et al., 2021), protect corals against pathogens (Welsh et al., 2017; Rosado et al., 2019; Ushijima et al., 2023), and increase coral calcification rates (Zhang et al., 2021) in laboratory trials, although none of these studies has evaluated the coral skeleton responses to microbiome manipulation. Here, we evaluated the structural properties of skeleton fragments of the shallow-water colonial scleractinian *Pocillopora damicornis* (Linnaeus, 1758) submitted to thermal stress and inoculated with *Vibrio coralliilyticus* (Ben-Haim et al., 2003) and BMCs in a mesocosm experiment searching for interactions of these forcings at the skeletal level. We also analyzed the crystal morphology, i.e., the aspect of aragonite crystal growth on the coral skeleton surface fibers and the elemental chemistry of the spine stem and tips.

2 Methods

2.1 Preparation of coral fragments

Three healthy colonies of the coral *Pocillopora damicornis*, 15–20 cm high, were obtained from four different aquarists in Brazil and fragmented after acclimation in coral tanks. A protocol was used to avoid potential contamination by exogenous microorganisms. Briefly, the coral colonies were cut for the mesocosm experiment using gloves, masks, and sterile materials. The use of artificial seawater (OceanTech®) also helped to prevent external contamination. Coral fragments 2–3-cm long were cut from the colony branches and then attached with quick-drying glue (Super Bonder) to small tiles (2.5 cm × 2.5 cm). Only the tips of the skeleton spine fragments were used for all analyses, and the density of the stems was measured for comparisons.

Healthy corals were described based on the Coral Color Reference Chart (Siebeck et al., 2006; Horvath et al., 2016), as well as on the F_v/F_m rates (Ralph et al., 2005). Both approaches can be proxies for coral holobiont health since color is related to its pigment and F_v/F_m to its vitality. These approaches were validated for *P. damicornis* corals by Rosado et al. (2019), as was the beneficial role of the BMCs used here (regarding mitigation of bleaching effects).

2.2 Mesocosm system design and components

The mesocosm system used in this study has been described previously (Rosado et al., 2019), although our experiment lasted longer (see Supplementary Figure S1). Briefly, the experiment was carried out between 22 October and 10 December 2016, i.e., for 50 days (Figure 1), including the acclimatization period. The experiment (first day) was considered to begin after 5 days of adaptation of *P. damicornis* colonies acquired from the aquarists' conditions (not shown in Figure 1). The mesocosm contained 24 1.5-L aquaria (15 cm × 11 cm × 12 cm, in trapezoidal format), arranged in two larger rectangular glass aquaria used as water baths (see Supplementary Figure S1). The rectangular water baths were supported by a wooden base 90 cm high, 50 cm wide, and 410 cm long with side-mounted shelves. Each small aquarium was equipped with a 26-L white plastic tank on the shelves, functioning as a sump, which was filled with 10 L of water. Each aquarium was connected by a 30-cm-long hose to its own sump; a 250-mL min^{-1} aquarium pump (Sarlo Better Mini A Pump) provided water circulation by pumping water through small silicone hoses from the sump to the
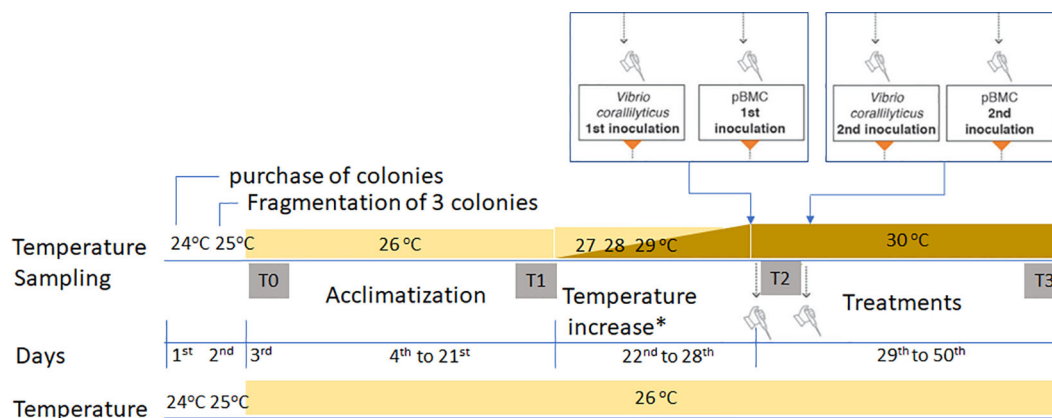
FIGURE 1
Mesocosm schedule, showing the acclimatization period, after which the temperatures were increased by 1°C/day, before the insertion of the microorganisms at different temperatures. T_0, the beginning of the experiment; T_1, sampling after the acclimatization period; T_2, no coral fragments were collected. This time represents the 28th day of the experiment when the temperature reached 30°C, and the inoculations of *V. coralliilyticus* and BMC were carried out in two rounds of inoculation, one when it reached 30°C and another 5 days later, always *Vibrio* first and BMC 1 day after. T_3, sampling from control treatments (CTL26 and CTL30), pathogen (P26 and P30), BMC consortium (C26 and C30), and pathogen + BMC consortium (PC26 and PC30). All treatments were sampled in quadruplicate. The asterisk indicates no temperature increases in the 26°C control experiment.

aquarium. Each aquarium had a 15-mm-diameter hole on top to allow a hose to be connected to the sump, and water was circulated in a closed system between the sump and the aquarium (see Supplementary Figure S1). An HG-370 air turbine was used to provide air to each aquarium through a silicone hose, which had its own controller to adjust airflow into the aquarium.

Two 100 and two 150-W Atman electric heaters were placed in each water bath to maintain a constant water temperature of either 26°C or 30°C. The temperature was controlled by an MT-518RI Full Gauge Digital Controller connected to the thermostats. Cold water came from a 1,000-L freshwater tank where the water was maintained at 18°C–19°C by a 3/4 HP chiller (Gelaqua, Santos, Brazil). Submersible Sarlo Better 2,000 L/h pumps were placed inside the 1,000-L cool-water tank to drain the water into the baths. Depending on the required water temperature in the bath, the controller switched the pumps or heaters on or off so that the temperature remained constant during the study. The water in each water bath was circulated and kept uniform by two SB 1000A aquarium pumps (Sarlo, São Paulo, Brazil). Artificial seawater (OceanTech®) with a salinity of 34 to 35 was used during the experiment.

The experiments took place under natural light. To control light exposure to the corals, a 70% shade cloth was placed above the mesocosm's polycarbonate roof, limiting light intensity to 250 μmol m^{-2} s^{-1} at noon, matching the natural environment. The mesocosm's north–south orientation replicated the coral's natural photoperiod and open-sky exposure. Four treatments at two different temperatures (26°C and 30°C) were used: I, control (CTL, without BMC or *Vibrio coralliilyticus* pathogen inoculation); II, BMC consortium (C, BMC inoculation only); III, pathogen (P, *V. coralliilyticus* inoculation only); and IV, pathogen + BMC consortium (PC, inoculation of both consortium and pathogen). For density analysis, the experiment utilized only the same coral genotype. However, for all other analyses, three independent coral colonies (genets) were used (Baums et al.,

2019), which were fragmented and randomly distributed. Treatments were performed in quadruplicate, and each aquarium was completely independent of the others, with each having its own sump and sharing only the water bath.

The mesocosm trial was started 1 day after the three coral colonies were fragmented and prepared to be distributed in the aquaria. The corals were not fed during the experiment. The trial included an 18-day acclimatization period, during which the water temperature in both water baths was maintained at 26°C. The variable that determined the end of the acclimatization period was the maximum PSII quantum yield (F_v/F_m). After 18 days, the water temperature was raised by 1°C per day in one of the water baths until reaching 30°C, to assess how high temperatures impact random coral skeletons between different treatments (Rosado et al., 2019). At the end of the experiment, 24 samples (three coral fragments per treatment, at two temperatures, 26°C and 30°C) were taken. All coral samples were placed in liquid nitrogen and sent for analysis.

2.3 Physicochemical parameters of water

During the mesocosm experiment, the physicochemical parameters of the seawater (pH, dissolved oxygen, and salinity) were measured daily in each aquarium to avoid possible confounding factors, such as pH (through constant monitoring), phosphate and nitrate concentrations (through constant water changes), natural irradiance (with intensity adjustment, using a shade cloth), O$_2$ content (maintaining the water saturated), salinity (maintained at 34–35 through regular measurements and water changes), and frequent water samples to identify method artifacts.

The results of seawater monitoring in the treatments ($n = 3$ per treatment) (Rosado et al., 2019) showed no considerable variation in any of the factors analyzed (salinity, which remained at 34–35 ppt; pH, maintained at 8.05–8.1; and dissolved oxygen, at 6.2–6.4 mg/L (at 26°C) and 5.7–6.0 mg/L (at 30°C) for all treatments.

Phosphate, ammonium, and nitrate levels remained homogeneous among treatments due to the artificial seawater used. Every 2 days, around 10% of the volume of each aquarium was replaced. Because there were no important differences between the data from any experiment indicating consistency in the controlled water conditions, these variables were not considered in this analysis.

2.4 Microbial assemblage

2.4.1 Ethics and permit approval

The microbial survey permit was obtained from SISGEN (Number A620FE5).

The cells of the pathogen *V. coralliilyticus* and the microbial consortium were prepared, maintained, and applied for this mesocosm.

Our analysis and data are from samples obtained in parallel but from the same experiment used by (Rosado et al., 2019), where all the details of the mesocosm are provided.

Briefly, each of the seven BMC strains [five *Pseudoalteromonas* spp., one *Cobetia* sp., and one *Halomonas* sp., all validated and described by Rosado et al. (2019)] were grown separately from the glycerol stock kept at −80°C. All seven strains reached 3.5×10^6 viable cells mL^{-1} 28 h after inoculation in 100 mL of MB medium. Cultures were centrifuged ($5,000 \times g$ for 2 min), and pellets were washed three times in NaCl (0.85%), followed by centrifugation ($5,000 \times g$ for 2 min). Pellets were then resuspended in 30 mL of NaCl (0.85%), reaching the concentration of 10^7 viable cells mL^{-1}. A mixture of 30 mL of NaCl (0.85%) solutions of each pBMC (resulting in a total volume of 210 mL) was produced, containing 10^7 cells mL^{-1} of each isolate. The pathogen used, *Vibrio coralliilyticus* (VC) strain YB (DSM19607), obtained from Deutsche Sammlung von Mikroorganismen und Zellkulturen GmbH (DMSZ, Germany) and stored in 80% glycerol at −80°C was recovered and grown on MA medium at 28°C for 16 h to reach a concentration of 10^5 viable cells mL^{-1}. Both the pathogen and BMCs, when inserted, were inoculated twice during the experiment.

2.5 Coral tissue removal

Samples were taken from the mesocosm and preserved in nitrogen. Before removing the tissue, they were placed in a freezer at −20°C for 15 min to slowly increase their temperature, and they were photographed at scale, without flash, on both sides, with careful observation of tissue distribution. To remove coral tissue and recover the skeleton free of trace elements that could bias elemental analysis, coral fragments were aerated with the Airbrush Double Action BD-134 K with the density cup, needle 3, 30 psi pressure, and an aqueous solution of 0.065 M phosphate buffer, pH 6.65 (Dove et al., 1995). The coral was manipulated with nitrile gloves and held with the fingers (tweezers damage the skeleton). It is important that the coral tissue is thawed while everything is done as rapidly as possible to avoid degradation of products due to prolonged exposure to ambient temperature stress.

After the tissue was removed, the coral skeleton cleaning procedure was performed: in a 15-mL Falcon tube, the samples were immersed in methanol (100%) (Barker et al., 2003) and placed in a freezer at −5°C for 60 min. The skeleton was then removed and placed in a 1% sodium hypochlorite solution (Fantazzini et al., 2015) for 3 days, then washed with distilled water and dried in an oven at 40°C for 3 days to perform mineralogical and structural analyses.

2.6 Physicochemical analyses

2.6.1 X-Ray diffraction

The X-ray diffraction (XRD) analyses were carried out with an X-ray diffractometer (Bruker D8 Advance with Lynxeye Detector), using Bragg–Brentano geometry and Cu Kα radiation (LDRX-UFF). XRD data were collected within the range 2θ of 3° to 100° with a step size of 0.0194° (2θ) and a counting time of 0.1 s per step. The crystalline structures were identified using DIFFRAC.SUITE EVA® and tables (Brindley and Brown, 1980).

2.6.2 Structural properties (porosity, median pore-size diameter, and density) in *Pocillopora damicornis*

Porosity and median pore-size diameters were analyzed by microtomography using a VersaXRM-510 microtomograph. The equipment consisted of a detector (CCD camera) placed diametrically opposite the X-ray source, with an adjustable voltage and electric current. The μ-CT has an X-ray source with a voltage of 0–160 kV and electrical power from 0 to 10 W, with a spatial resolution of up to 0.9 μm. An objective lens with optical and geometric magnification of up to ×40 was also used. The images were acquired by a detector with 1,024 pixels × 1,024 pixels. A power source of 80 kV, 7 W, with a resolution of 5 μm was used with all the equipment. The μ-CT data were recorded as 2D projections ("slices") at various angles. 3D images (tomography) of the coral were generated using these slices. Each tomogram was 300 voxels × 300 voxels × 300 voxels with a 5-μm voxel size. The software Avizo Fire® was used to characterize coral skeletal components and generate 3D coral images to obtain the porosity and estimate the median pore-size diameter (MPSD). The Avizo porosity data results are a simulation for estimating porosity based on pore-size distribution. The estimate and the porosity data are shown by the program (including the lowest to the highest values), which are determined by the resolution of the analysis and pixel size. Each simulation performed ($n = 3$) was added and divided by the number of simulations for each coral fragment, obtaining the mean porosity.

One estimate will never be the same as another, as it will depend on the estimated area of interest, the voxel size scanned, the manipulation of the images, and the heterogeneity of the corals. In the image treatment, smoothing filters were selected, possible attenuations were corrected, and the threshold was adjusted in the gray scale.

The bulk density (g/cm^3) results from the pattern in which the mineral is laid down (the meso-architecture) and the volume of skeletal voids that it encloses (Bucher et al., 1998). The bulk density

was obtained from the XRD mineralogical analysis and the µCT structure data through the formula:

$$Bulk\ density\ =\ micro\text{-}density\ *\ (1-porosity)$$

Where micro-density is the specific gravity of the material comprising the skeleton (obtained from XRD analysis).

To minimize genetic variability and enable comparison of density across different experiments, only fragments of *P. damicornis* ($n = 1$) with identical genotypes were used for analysis of the mean density in skeletogenesis. All other analyses were performed using the three different phenotypes from distinct sources, as described previously. The skeleton mineral density (SMD, g/cm^2) and skeleton mineral content (SMC, g^{-2}) represent the surface mineral calcification calculated for each sample by comparing against the densitometer internal standard for calcium carbonate (Braz et al., 2022). Each piece was marked with two regions of interest (ROIs) of 0.5–0.6 cm. The two regions of interest were marked as the stem and the tip of the piece, corresponding to the analyses before and after treatment, respectively. The superficial skeleton density analysis was carried out using the iDXA-Lunar model equipment, enCORETM 2008 software, version 12.30 (GE Healthcare$^®$).

2.6.3 Energy-dispersive X-ray spectroscopy and scanning electron microscopy

The energy-dispersive X-ray spectroscopy (EDX/scanning electron microscopy (SEM)) analysis for the coral samples was done using a Hitachi TM 3000 tabletop environmental scanning electron microscope to determine the chemical element composition and relative contents of each chemical element on the surface of the coral skeleton fibers before gold coating. Measurements were taken at a high-vacuum setting with an accelerating voltage of 15 kV, a beam current of ~7 nA, and an acquisition time of 120 s, and results were compared for all treatment options. Three points on any fragment are enough to measure elements by EDX (Isa, 1986). However, we chose five areas to measure the element composition of the tip and five of the stems ($n = 20$ for each treatment), and the results are expressed in millimoles/mole.

The morphology of the apical corallites and septa of the samples were analyzed using SEM photomicrographs. All samples from treatments T_0 and T_3 (27 coral fragments) were prepared to study their three-dimensional skeletal micro-morphologies (coral fibers). Tips of the spine of coral samples ranging from 3 to 5 mm long were carefully removed from the apical branches of *P. damicornis* to observe the skeletal morphology of the coral septa (Brown et al., 1983). Samples were studied at magnifications between ×2,000 and ×20,000. Skeletal micro-morphology in septa of different corallites was studied and compared within and between the treatments (Brown et al., 1983; Stolarski, 2003; Nothdurft and Webb, 2007). Coral samples for SEM observations were embedded in Araldite 502/Embed 812 resin to enable cutting into fine sections in all directions, with an Extec Labcut$^®$ 150 Microtome diamond saw to enhance skeleton observation. Due to the fragile nature of coral fragments under the microtome, they are likely to be crushed during cutting unless they are embedded in epoxy resin. The resin allows the coral samples to be cut into the required forms and sizes. Sections of coral lamina at 1 mm thick were prepared and placed on a metal support covered with carbon tape to hold the specimens. In addition to the prepared specimen, a small section of each coral tip, 3–5 mm long was harvested without preparation. These sections were placed on the metal support to confirm that the preparation process had no secondary effect on the coral micromorphology. The samples were sputter-coated with gold 20 nm thick for 180 s to prepare them for SEM observations.

The septa were selected as the region for further analysis of micromorphology, in which the coral corallite, spine, septa, thecal walls, and costae are the most active sites for crystal formation (Cohen and McConnaughey, 2003). The surface morphologies of coral fibers in the skeletal septa of *P. damicornis* were compared. The septa in three coral fragments subjected to each treatment were investigated in apical and lateral views.

2.7 Statistical analysis

Statistical analysis was performed using software R v 4.1. (Hair et al., 2010; R Core Team, 2020; Denis, 2021) and Statistica 10.0 StatSoft package (Developer:StatSoft). Data from each variable were tested for homogeneity of variance within each treatment, using Levene's test (leveneTest function in the "car" package), and data were statistically tested for normality using Shapiro–Wilk test (Shapiro.test function in the "stats" package). Among branch tips, a three-way ANOVA was used to test the interaction between temperature, BMC, and pathogen inoculation. A two-way ANOVA was applied to the database to determine differences in skeleton between the two temperature conditions (26°C and 30°C), followed by a Tukey's *post-hoc* test at the 95% confidence level. To determinate differences between structures calcified before (e.g., stems) and after (i.e., tips) the experiment, paired *t*-tests were used with effect sizes reported as Cohen's *d* ($d = 0.2$: small effect; $d = 0.5$: medium effect; $d = 0.8$: strong effect). Data were plotted (ggplot function in the "ggplot2" package) and combined (plot_grid function in the "cowplot" package) in R. Data cited in the text refer to mean ± standard deviation (SD).

3 Results

3.1 Skeleton properties of *Pocillopora damicornis*

No main and interactive effects between temperature, consortium, and pathogen application were detected in skeletal mineral density (SMD) among structures calcified during the experiments (i.e., among tips) (three-way ANOVA, Supplementary Table S1). However, for skeletal mineral calcification (SMC), a significant effect of pathogen was observed (two-way ANOVA, $p = 0.03$, $F = 5.8$, $df = 1$), and skeletal mass was higher (two-way ANOVA, $p = 0.04$, $F = 4.4$, $df = 3$) in thermally stressed corals that were inoculated with both the pathogen

and BMC, compared to the control conditions (Tukey's *post-hoc* test, $p = 0.04$; Supplementary Figure S2).

Significant differences were also observed when comparing the structures calcified before (i.e., stems) and during the experiment, as shown in Figures 2A, B. Concerning SMD, a significant decrease was observed in thermally stressed corals inoculated with *V. coralliilyticus* (Figure 2A, treatment P30, 0.90 g/cm² ± 0.22 g/cm² to 0.66 g/cm² ± 0.10 g/cm², p-value = 0.01, Cohen's $d = 1.39$).

For skeletal mineral calcification (SMC), significant decreases in skeletal mass were observed in the control at high temperature (Figure 2B, treatment CTL30, 0.043 g^{-2} ± 0.006 g^{-2} to 0.027 g^{-2} ± 0.006 g^{-2}, $p = 0.03$, Cohen's $d = 2.88$) and when the pathogen was inoculated (treatment P30, 0.052 g^{-2} ± 0.01 g^{-2} to 0.036 g^{-2} ± 0.005 g^{-2}, $p = 0.01$, Cohen's $d = 1.6$). When BMC was inoculated, however, no significant changes were observed in either SMD (treatment C30, p-value = 0.16, Cohen's $d = 1.79$; treatment PC30, p-value = 0.18, Cohen's $d = 1.08$) or SMC (treatment C30, $p = 0.1$, Cohen's $d = 2.12$; treatment PC30, $p = 0.3$, Cohen's $d = 0.84$).

For branch tips (Figures 3A–C), the X-ray micro-CT analysis revealed that the median pore-size diameter (MPSD, Figure 3B) differed significantly in coral fragments kept at both low (Kruskal–Wallis test, Chi-square value = 255.12, $df = 3$, p-value = > 0.01) and high temperature (Kruskal–Wallis test, Chi-square = 50.44, $df = 3$, p-value< 0.01). Compared to the control (26°C), inoculation of both BMC (Dunn's *post-hoc* test, p< 0.01, $z = 7.6$) and pathogen (Dunn's *post-hoc* test, p< 0.01, $z = -15.1$) increased the pore diameter in *P. damicornis*, with the highest (median: 172.8 μm) and lowest (median: 61.8.7 μm) sizes measured in coral fragments from treatments P26 and CTL26, respectively (Figure 3B). Under high temperatures, however, pore sizes were smaller in corals inoculated

with BMC (treatment C30; median: 16.9 μm), with significant changes (Dunn's *post-hoc* test, p< 0.01, $z = -4$) detected only in corals inoculated with the pathogen plus BMC (treatment PC30; median: 135.2 μm), which showed the highest values.

Based on pore-size distribution (Figure 3B), the estimated porosity (Figure 3C) was highest in pathogen-challenged coral fragments in both low (treatment P26, 47.33% ± 6.66%) and high temperature (treatment P30, 39.33% ± 13.80%) experiments. The lowest levels were observed in the control samples at 26°C (treatment CTL26, 21.67% ± 4.62%) and when BMC was inoculated at 30°C (treatment C30, 37% ± 5%). The specific gravity of the coral skeleton aragonite, hereafter termed microdensity (or real density), was 2.93 g/cm³ in all treatments, and the coral skeleton solids ranged from 0.52% to 0.78% among treatments. Results for density, porosity, and MPSD are reported in Supplementary Table S2 and statistical comparisons in Supplementary Table S1.

3.2 Crystal morphology in coral skeletons through SEM microphotographs

Laminar aragonite crystals were identified in the coral skeletons in all treatments (Figures 4, 5). The coral fibers in all parts of the septa were dense and compact in all treatments, with approximately the same size and form (Figure 4A). Coral fiber morphologies in the septa in both temperature treatments resembled the coral purchased from the aquarist (pattern: T_0; Figure 4A). Four types of morphologies were observed on the coral skeleton surface and differed among the treatments (Supplementary Table S3).

FIGURE 2
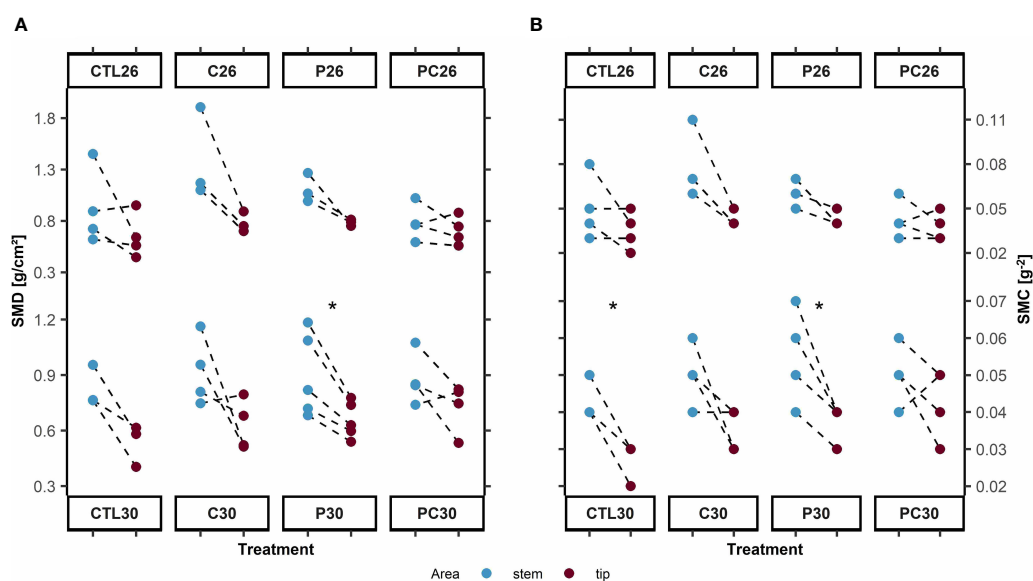**(A)** Skeleton structure of stem and branch tips of *Pocillopora damicornis* based on skeleton mineral density (g/cm²) and **(B)** skeletal mineral content (SMC, g⁻²) under treatments: Control, C = BMC consortium, P = Pathogen *Vibrio coralliilyticus*, and PC = Pathogen and BMC, at temperatures of 26 and 30 °C. *denotes p < 0.05.
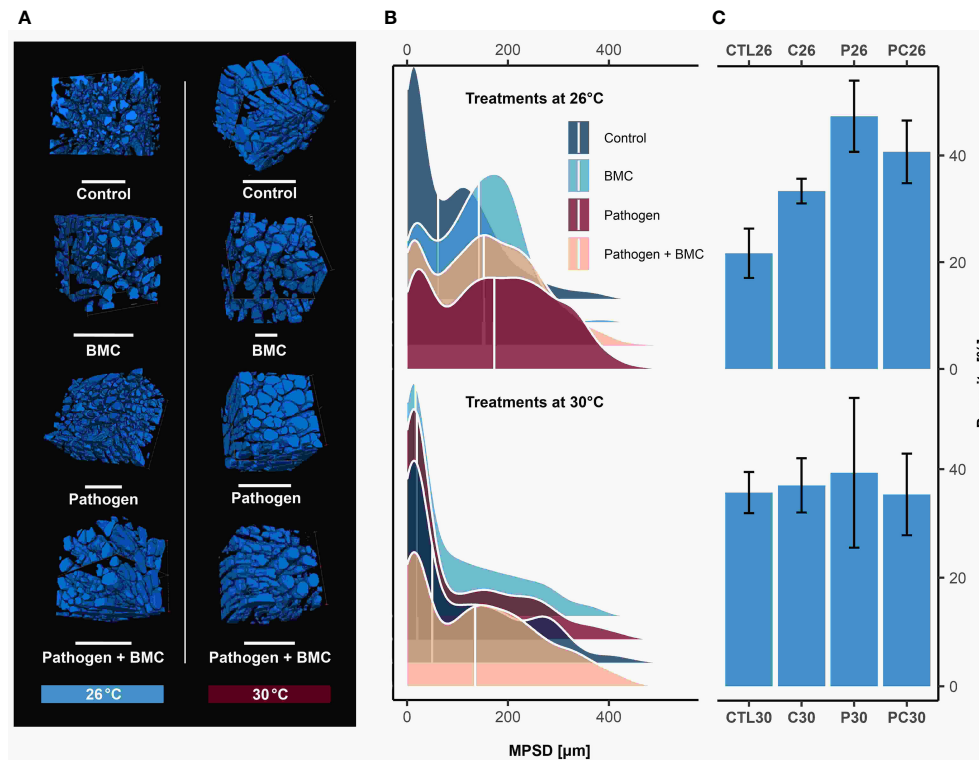
FIGURE 3
(A) The 3D volume rendering of coral branch tips of *Pocillopora damicornis* analyzed in μ-CT. Empty spaces (pores) are shown in blue. Scale bars measure 1 mm. **(B)** Density plot of pore-size diameter under treatments of control, BMC, pathogen *Vibrio coralliilyticus*, and pathogen and BMC (P + BMC); n = 3 for each treatment. The white line indicates median values. **(C)** The skeleton structure of *P. damicornis* based on branch-tip porosity (mean ± SD).

SEM observations of coral skeletons during treatment with BMC at 26°C and 30°C showed two morphologies (laminar and granular). In the other treatments (T_0, control: 26°C, control: 30°C, pathogen: 30°C, and BMC plus pathogen: 30°C), three-dimensional *c*-axis direction aragonite crystals formed a cluster of fibers, while the dominance of granular morphology was observed toward the top of the skeletal structure (Figure 4). Crystalline borders and edges between the fibers were highly compacted (Figure 5). Treatment with the pathogen and BMCs at 26°C showed two crystal habits, one of which (spherulitic) differed among the treatments (T_0, control, and pathogen). For most treatments at 30°C, three morphologies (laminar, granular, and acicular) were observed in the coral skeletons (Figures 4D, E, 5A, D; Supplementary Table S3).

Laminar fibers, with slight differences in shape (Figures 4A, B), were observed with a curvature in some fractured septa; in general, these fibers were abundant in the control samples kept at 26°C. Spherulitic morphology can be seen in Figure 5E.

3.3 X-ray diffraction

As expected, only aragonite was observed in the crystalline structure of the coral samples in the different treatments. Therefore, 2.93 g/cm^{-3} was used to calculate the variability of thickness and spacing of a skeleton volume, i.e., bulk-density values.

3.4 The Sr/Ca and Mg/Ca ratios of *Pocillopora damicornis* surface skeleton

To evaluate element incorporation, the mean Sr/Ca and Mg/Ca ratios between the stem and coral tips were compared.

Element incorporation was considerably affected by increases in temperature, BMC, and pathogen inoculation (Figure 6; Supplementary Table S1, S4). Among treatments, coral Sr/Ca ratios were relatively more stable (mean range: 13.42–18.5 mmol/mol) compared to Mg/Ca ratios (mean range: 0–48.2 mmol/mol). Regarding Sr/Ca ratios, a three-way ANOVA indicated a significant effect of temperature ($p = 0.035$, $F = 4,860$, $df = 1$) and interactions of temperature × BMC × pathogen among the coral branch tips that calcified during the experiment ($p = 0.0048$, $F = 9,219$, $df = 1$). Notably, pathogen inoculation increased Sr incorporation at 30°C in corals not inoculated with BMC (treatment P30, Sr/Ca = 17.3 mmol/mol) compared to the control (treatment CTL30, Sr/Ca = 14.1 mmol/mol). However, these differences were only marginally significant (Tukey's *post-hoc* test, $p = 0.05$) and were dependent on temperature, observed exclusively in thermally stressed corals (two-way ANOVA, $p = 0.01$, $F = 8.1$, $df = 1$) (Supplementary Figure S2).

When comparing stem and branch tips of the same individuals, significant differences in Sr/Ca ratios were only detected in corals inoculated with both pathogen + BMC at low temperature (treatment PC26, 18.5 mmol/mol ± 2.2 mmol/mol to 14.3 mmol/mol ± 2.4 mmol/mol, $p = 0.008$, Cohen's $d = 2.31$).
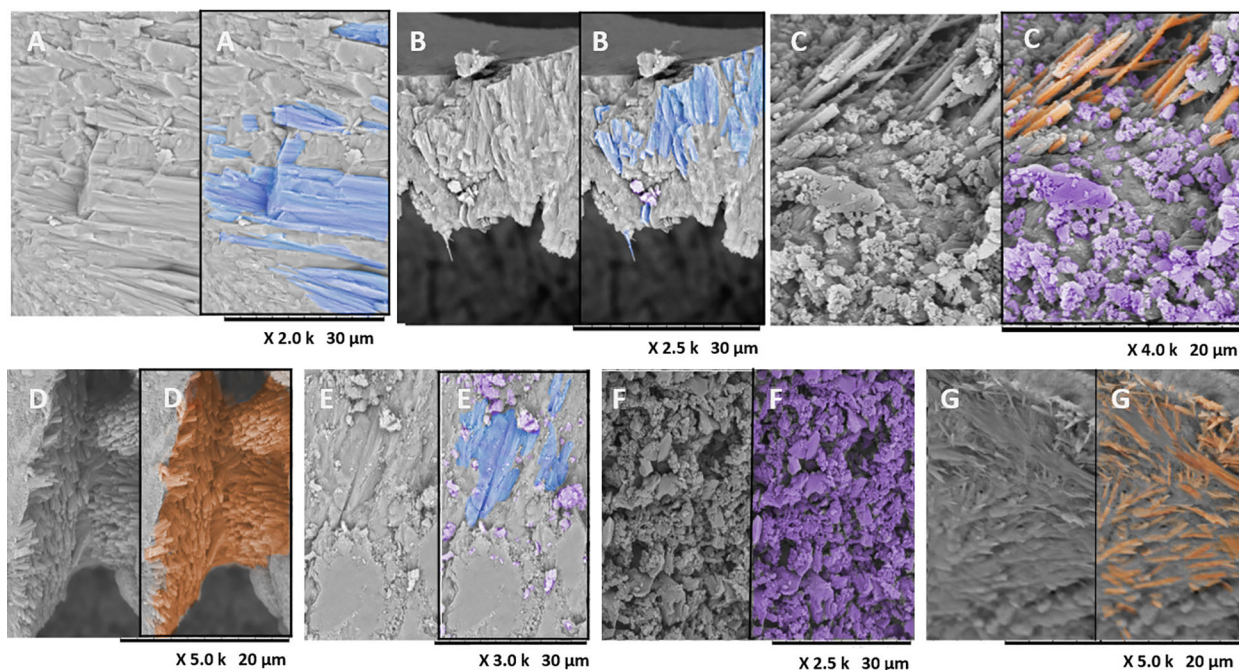
FIGURE 4
SEM photomicrographs of the lateral wall of sclerodermites. **(A)** Laminar aragonite crystals (blue) forming a cluster of skeletal fibers in *Pocillopora damicornis* with no treatment (T_0). **(B)** Morphology in the control at 26°C, showing similar laminar fibers **(A, B)**. **(C)** SEM photomicrograph of corallite morphology in *P. damicornis* in the control at 30°C, showing newly formed aragonite acicular crystals (orange) with a granular habit (purple) in the septa. **(D)** Micro-morphologies of a calcifying interface, showing matrix fibrils with an agglomerated, thickened, nonpointed acicular micro-morphology in septa of the corallites of *P. damicornis* in the treatment with the pathogen at 26°C. **(E−G)** SEM photomicrographs of the corallites of *P. damicornis* with the pathogen at 30°C. **(E)** Laminar fibers; **(F)** granular habit in septum; **(G)** aragonite acicular habit in septum fragment.

Concerning Mg/Ca ratios, the three-way ANOVA indicated significant effects of temperature ($p < 0.01$, $F = 111$, $df = 1$) and pathogen inoculation ($p < 0.01$, $F = 123$, $df = 1$), as well as a significant interaction between temperature x pathogen ($p < 0.01$, $F = 523$, $df = 1$) and pathogen × BMC ($p < 0.01$, $F = 375,557$, $df = 1$) on coral branch tips.

Specifically, at a temperature of 26°C, corals inoculated with BMC (treatment C26) exhibited lower Mg uptake (Tukey's post-hoc test, $p = 0.01$, Mg/Ca = 14.3 mmol/mol ± 10 mmol/mol) compared to corals maintained under control conditions (CTL26, 27.8 mmol/mol ± 2.7 mmol/mol).

At 30°C, Mg incorporation was highest in corals inoculated with both pathogen and BMC (treatment PC30, 42.1 mmol/mol ± 4.6 mmol/mol) with respect to all other treatments: CLT30 (Tukey's post-hoc test, $p < 0.01$, 19.4 mmol/mol ± 3.5 mmol/mol), P30 (Tukey's post-hoc test, $p < 0.01$, 27 mmol/mol ± 4.6 mmol/mol), and C30 (Tukey's post-hoc test, $p < 0.01$, 12.7 mmol/mol ± 2.1 mmol/mol). Additionally, the incorporation of Mg was also significantly higher in corals inoculated with pathogens (Tukey's post-hoc test, $p < 0.01$, 27 mmol/mol ± 4.6 mmol/mol) than with BMC (12.7 mmol/mol ± 2.1 mmol/mol).

Comparing stem and branch tips (Figure 6), significant differences in Mg/Ca ratios were also detected after BMC inoculation at high temperatures; specifically, BMC improved calcium uptake (treatment C30, 17.7 mmol/mol ± 1.3 mmol/mol to 12.7 mmol/mol ± 2.1 mmol/mol (stems to tip), $p = 0.003$,

Cohen's $d = 1$) compared to previously precipitated structures (stems). On the other hand, when the pathogen was inoculated at 26°C, calcium decreased in the skeleton, as evidenced by the Mg/Ca increase at the tips (treatment P26, 0 mmol/mol ± 0 mmol/mol to 10.7 mmol/mol ± 0.8 mmol/mol, $p = 0.000$, Cohen's $d = 17.9$).

No significant changes were detected in treatments CTL26, C26, PC26, CTL30, P30, and PC30, with the lowest variation observed in corals kept in the control (CTL) in the low-temperature regime (treatment CTL26, 28.6 mmol/mol ± 3.5 mmol/mol to 27.8 ± 2.7 mmol/mol, $p = 0.8$, Cohen's $d = 0.24$).

4 Discussion

Bacterial communities associated with corals, together with endosymbiotic members of the family Symbiodiniaceae (Morgans et al., 2020), have important roles in coral health, calcification, and life cycles (Rohwer et al., 2002; Lesser et al., 2004; Peixoto et al., 2017; Peixoto et al., 2021; Voolstra et al., 2021). These bacterial communities can be found in the coral tissue (Lesser et al., 2004; Koren and Rosenberg, 2006; Pollock et al., 2018), mucus (Rohwer et al., 2002; Ritchie, 2006; Kooperman et al., 2007; Pollock et al., 2018), skeleton (Yang et al., 2016; Pollock et al., 2018; Ricci et al., 2019; Pernice et al., 2020), and gastric cavities (Herndl and Velimirov, 1985; Agostini et al., 2012; Pernice et al., 2020; Zhou
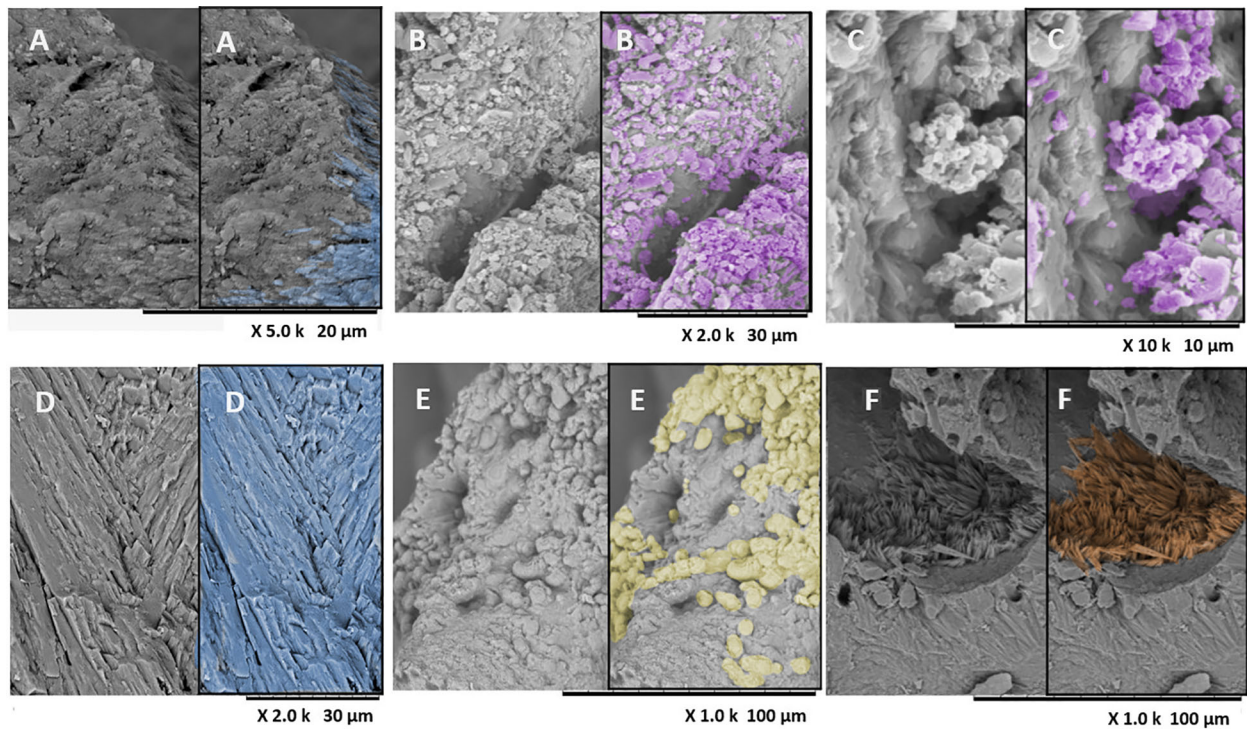
FIGURE 5
SEM photomicrographs of corallite morphology in *Pocillopora damicornis* with BMC at 26°C. **(A)** Transverse section in apical view of the coral spine showing laminar fibers (blue) of *P. damicornis*. **(B, C)** SEM photomicrographs of corallite morphology in *P. damicornis* with BMC at 30°C, showing granular habit (purple). **(D, E)** SEM photomicrographs of the corallites of *P. damicornis* in the treatment with the pathogen plus BMC at 26°C. Morphologies in corallites: **(D)** the laminar fibers; **(E)** the spherulitic fibers (yellow), which were found only in BMC + pathogen at 26°C; **(F)** SEM photomicrograph of the corallites in *P. damicornis* in the treatment with pathogen plus BMC at 30°C, showing aragonite crystals of acicular habit (orange) in septa fragment.

et al., 2020). The bacterial communities are sensitive to environmental parameters and can quickly react to environmental shifts (Voolstra and Ziegler, 2020), affecting coral physiology and health (Bourne et al., 2016).

The use of BMCs (Peixoto et al., 2017), together with the ability of the coral holobiont to restructure its microbiome (Voolstra and Ziegler, 2020; Voolstra et al., 2021), comprise a manipulative solution to restore and rehabilitate damaged microbiomes and
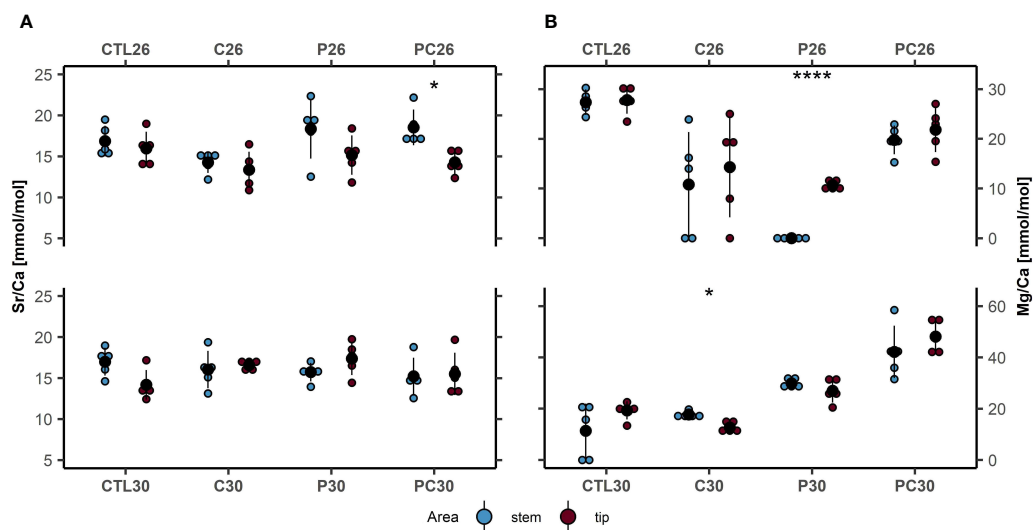
FIGURE 6
(A) Ratios of Sr/Ca (mmol/mol) and **(B)** Mg/Ca (mmol/mol) in the coral skeleton branch stem (blue) and tips (red) of *Pocillopora damicornis* under different temperature treatments and control (mean ± SD, *n* = 5 for each treatment): CTL, control; C, consortium of BMC; P, pathogen *Vibrio corallilyticus*; PC, pathogen and BMC. ****$p < 0.0001$; *$p < 0.05$. Black dots and lines are mean + SD values; colored dots are bulk values.

promote coral health and growth (Rosado et al., 2019; Zhang et al., 2021; Peixoto et al., 2022; Peixoto and Voolstra, 2023). In mesocosm trials, the BMC consortium has been efficient in mitigating visual and physiological bleaching effects caused by both thermal stress and pathogen challenge (Rosado et al., 2019). Although the present experiment was conducted in the same mesocosm used by these last authors, the focus here was on the physical properties, micro-morphological responses, and elemental composition of the skeleton to BMC and pathogen inoculation. BMC could influence fiber morphology and porosity (Cohen and McConnaughey, 2003; Meibom et al., 2004; Sinclair, 2005; Shirai et al., 2008; Roche et al., 2011), which are commonly used proxies for calcification and in response to heat stress (Hetzinger et al., 2016; D'Olivo and McCulloch, 2017).

The inhibition of photosynthesis at high temperatures can lead to reductions in calcification rate and skeletal density. One factor to consider is that the influence of temperature on calcification can be species-specific, with different responses among coral species. Furthermore, these differences can also be explained by clades of *Symbiodinium* sp. present in coral microbiota since some clades are more resistant to higher temperatures than others. Infection by *V. coralliilyticus* can cause a decrease in the density of zooxanthellae (bleaching), tissue lysis, and eventual death (Zhou et al., 2020). In our study, considerable decreases in skeleton density and calcification were observed in thermally stressed corals inoculated with *V. coralliilyticus* (Figure 3). The effect of BMC on the coral skeleton was evaluated, and no reductions in SMC and SMD at the stem and coral tips were detected in treatments with BMC and in BMC with the pathogen at 30°C (Figure 2); however, our results indicated that the consortium, when inoculated, can mitigate the effects of the pathogen *V. coralliilyticus* and even improve calcification at high temperatures at skeletal levels, coinciding with the promising results of other studies using microbial therapies to enhance coral health (Rosado et al., 2019; Doering et al., 2021; Santoro et al., 2021). At high temperatures, for example, a significant effect of pathogen was observed (two-way ANOVA, p = 0.03, F = 5.8, df = 1), but the skeletal mass of coral branch tips was higher in thermally stressed corals inoculated with both pathogen and BMC (treatment PC30, SMC = 0.043 g^{-2} ± 0.01 g^{-2}) than in thermal stressed control conditions (treatment CTL30, SMC = 0.027 g^{-2} ± 0.006 g^{-2}, Tuckey's *post-hoc* test, p = 0.04; Supplementary Figure S2).

Microorganisms have been shown to become integrated into the coral skeleton and act as additional support for their structure. The microbial influence on the structural integrity of the coral skeleton of *P. damicornis* has previously been described, through the symbiotic relationship with endolithic microalgae and fungal symbionts living inside the coral skeleton (Pernice et al., 2020). This unique symbiotic relationship seems to promote the fitness of skeletogenic cell types and increase the physical support of the skeleton of corals under stress (Domart-Coulon et al., 2004).

In this mesocosm, pH and nutrients were controlled to maintain a high aragonite saturation state constant in the calcifying site and oligotrophy. The correlation between higher porosity and a higher linear growth rate in regions with lower hydrodynamic energy (as in our mesocosm) has also been

described, showing that increased porosity could be interpreted as eco-physiological feedback (Mwachireya et al., 2016). An increase in porosity may occur in corals with no change in the micro-density of the skeleton (Bucher et al., 1998). In our experiment, comparison between structures calcified before and during the experiment revealed that porosity increased after inoculation of both the pathogen and BMC, but significant decreases of SMD (treatment P30, 0.90 g/cm² ± 0.2 g/cm² to 0.66 g/cm² ± 0.10 g/cm², p-value = 0.01, Cohen's d = 1.39) and SMC (treatment P30, 0.052 g/cm² ± 0.01 g/cm² to 0.036 g/cm² ± 0.005 g/cm², p = 0.01, Cohen's d = 1.6) were only correlated with inoculation of *V. coralliilyticus*, indicating the mitigative potential of BMCs (Figures 2A, B). Our data showed improvement in the coral skeleton health and growth caused by BMC inoculation, such as the maintenance of skeleton calcification properties (e.g., skeleton density), combined with the health improvements previously observed in the tissue (Rosado et al., 2019).

Coral skeletons are important for the ability of corals to repair damage from natural and unnatural erosion (Cameron and Edmunds, 2014; Pisapia and Pratchett, 2014). The resistance of coral to high hydrodynamic-energy events (hurricanes, ocean currents, etc.) is directly affected by coral skeletal quality (Spiske et al., 2008). The mean porosity (Figure 3C) found in corals from all our treatments (21.67% to 47.33%) is considered low to normal if compared to the mean porosity found for healthy *P. damicornis* (54.28%) (Walsh et al., 2012). Inoculation of BMCs at low temperatures seemed to increase both the pore diameter (treatment C26, Figure 3B, median 142 μm) and porosity (treatment C26, Figure 3C, 33.3% ± 2.3%) compared to the control (treatment CTL26, MPSD 61 μm; porosity 21.7% ± 4.6%), which could be correlated with an increase in calcification and linear extension. On the other hand, pathogen inoculation also seemed to increase porosity (treatment P26, 47.33 ± 6.66). In fact, the porosity of the coral skeleton alone is a fragile metric to evaluate coral health or skeleton strength, as it can be influenced by stress or growth (linear extension/calcification). It could, at the same time, indicate stress caused by the pathogen and increased calcification promoted by BMCs, as corals increase their porosity as a protective response to stress (Fantazzini et al., 2015). The coral-skeleton porosity can be influenced by phosphate levels, for example, by decreasing density and porosity (Bucher et al., 1998; Koop et al., 2001) and by increasing skeleton density (Takabayashi, 1996; Koop et al., 2001). Porosity can also be influenced by hydrodynamic energy, turbidity, and nutrients (Mwachireya et al., 2016) and may vary in different regions of the skeleton (Baldock et al., 2014). Skeletal strength cannot be measured by porosity alone and must also be assessed by the microdensity (real density) and density values (Bucher et al., 1998; Spiske et al., 2008; Dunn et al., 2012; Fantazzini et al., 2015). Corals increase their skeletal macroporosity (porosity > 10 μm) to maintain a constant linear extension in response to the reduction of skeletal mineralization at low pH, indicating that this process is beneficial for their reproductive performance (Fantazzini et al., 2015).

Aragonite crystal fibers newly precipitated during coral skeletogenesis can be observed directly through studies under controlled culture conditions by comparison of the fiber

morphology found at T_0 with the morphology at the end of the experiment, T_3 (Figures 4, 5). This is due to the rapid crystal growth in corals such as *P. damicornis* and the temperature-driven aragonite state of the calcifying fluid (Cohen and McConnaughey, 2003). During the initial phases of the treatments, skeleton surfaces with a laminar habit were common in all skeletons (Figures 4A, B). At the end of the mesocosm treatments, after the pathogen and the BMC were inoculated, both separately and together, granular morphology began to appear (Figures 4B, C) at both temperatures and spherulitic morphology at 26°C (Figure 5E). Spherulites result in high growth rates (Cohen and McConnaughey, 2003) because this mechanism of noncrystallographic crystal formation can adjust to fill spaces faster than any other aragonite geometry (Sun, 2017). The spherulite crystal morphology was possible because of the extremely rapid crystal growth, as evidenced by the Mg/Ca ratios, and could also be combined with the thickening of fibers (Sun, 2017). The match between this crystallographic orientation and the treatment with BMC together with the pathogen at 26°C leads us to direct attention to these structures, as they may represent the thickening of the skeletons. The probiotic microbiota represented by BMC and the pathogen could be influencing the organic matrix framework in skeletogenesis. The acicular habit (Figures 4C, G) was frequent in the treatments at 30°C with the control and pathogen, showing the effect of temperature on the isothermal coral system of *P. damicornis*, favoring the growth of aragonite needles. Clumps of granular aragonite crystals were precipitated in the calcifying space of the spines, where high Mg/Ca ratios were observed.

Vibrio coralliilyticus is a pathogen that negatively affects the zooxanthellae of corals at high temperatures (Ben-Haim et al., 2003; Cervino et al., 2004; Vezzulli et al., 2010). When *P. damicornis* is infected by *V. coralliilyticus* at temperatures higher than 27°C, the coral starts to bleach, and the zooxanthella concentration decreases to less than 12% of that in a healthy coral (Cervino et al., 2004). No studies have, however, investigated the effects of *V. coralliilyticus* on coral skeletons. Our results revealed that *V. coralliilyticus* can affect the composition of the *P. damicornis* skeleton, as well as the porosity, median pore-size diameter, and morphology. As previously established, any variation in nutrient levels in seawater can affect calcification processes, metabolism, and photosynthesis (Hofmann et al., 2013). Even considering these limitations and the significance of porosity when evaluated alone, the increased porosity may indicate damage to corals caused by *V. coralliilyticus*, even at low temperatures (26°C) and before any signs of stress are visible.

Interestingly, inoculation with the pathogen and BMC together seemed to mitigate the impacts caused by *V. coralliilyticus*. These results could be explained in two ways: either the inoculation of bacterial cells provides a heterotrophic source of nutrients (food) (Morgans et al., 2020), which is unlikely because of the negligible number of inoculated cells, or through other beneficial mechanisms of the BMCs are triggered or even amplified by in this case by the presence of the pathogen at high temperature. As *V. coralliilyticus* is pathogenic at 30°C and a considerable concentration of viable cells of *V. coralliilyticus* was detected in the same samples by qPCR only when corals were inoculated with *V. coralliilyticus* without BMCs at

30°C (Rosado et al., 2019), the second option appears more likely. This hypothesis was supported in the study by Santoro et al. (2021), in which BMC activity and function were triggered and tracked when corals were subjected to stress.

While no differences were observed in the artificial seawater used and the pH was controlled, the amount of calcium was higher on the skeletal surfaces of the corals inoculated with BMC compared to previously precipitated structures (stems) at 30°C (treatment C30, 17.7 mmol/mol ± 1.3 mmol/mol to 12.7 mmol/mol ± 2.1 mmol/mol (stems to tip), $p = 0.003$, Cohen's $d = 1$) (Figure 6). (26°C and 30°C, Figure 6).

These results indicated that BMCs could assist corals in depositing more calcium ions in their skeletons, which could also lead to the observed variations in the contents of minor elements and the previously observed higher photosynthesis rate in *P. damicornis* (Rosado et al., 2019). Calcium and, to a lesser extent, inorganic carbon are the two most important components for photosynthesis and calcification in *Scleractinia* corals (Cameron and Edmunds, 2014), and decreases in calcium levels in seawater inhibit photosynthesis in these corals (Spiske et al., 2008). While the putatively increased calcification rate needs to be confirmed, including by observations of other species, our preliminary results indicated that in *P. damicornis*, the calcium content was boosted by BMC inoculation (treatment C30, 17.7 mmol/mol ± 1.3 mmol/mol to 12.7 mmol/mol ± 2.1 mmol/mol (stems to tip), $p = 0.003$, Cohen's $d = 1$). These results align with other recent results (Zhang et al., 2021) indicating that BMCs increase *P. damicornis* calcification under normal temperatures and that this effect extends to thermally stressed corals. These results also support the hypothesis that BMCs can accelerate coral growth and calcification, which is an important aid in coral gardening and restoration efforts (Peixoto et al., 2022). Increased calcium incorporation at the calcification site has also been reported as a driver of increased coral resistance to ocean acidification (Walsh et al., 2012).

Despite its importance, calcium alone cannot control the calcification process, and ratios of trace metals and other elements also seem to affect coral growth (Herndl and Velimirov, 1985; Fantazzini et al., 2015; Pernice et al., 2020). Calcium, magnesium, and strontium are responsible for biomineral crystal formation in coral skeletons (Marshall and Clode, 2004; Mass et al., 2017), and any change in calcium composition seems to affect the shape of crystalline structures (fibers) in coral skeletons, as well as biomineralization processes (Roche et al., 2011). The ratios of Li/Ca, Na/Ca, and Mg/Ca, for example, define growth rates and skeletal quality in scleractinian corals and are influenced directly or indirectly by temperature (Rollion-Bard and Blamart, 2015). Here, a three-way ANOVA indicated the significant effect of temperature (three-way ANOVA, $p = 0.035$, $F = 4,860$; $df = 1$) and the interactions of temperature × BMC × pathogen in Sr/Ca ratios among *P. damicornis* skeletons under the different treatments (three-way ANOVA, $p = 0.0048$, $F = 9,219$, $df = 1$). However, differences were only marginally significant (Tuckey's *post-hoc* test, $p = 0.05$; Supplementary Figure S2), which could confirm the influence of the partitioning coefficient (Kd) model of metal cations in aragonite (Inoue et al., 2007). Among branch tips,

three-way ANOVA indicated significant effects by temperature (three-way ANOVA, $p < 0.01$, $F = 111$, $df = 1$) and pathogen inoculation (three-way ANOVA, $p < 0.01$, $F = 123$, $df = 1$), as well as a significant interaction between temperature × pathogen (three-way ANOVA, $p < 0.01$, $F = 523$, $df = 1$) and pathogen × BMC (three-way ANOVA, $p < 0.01$, $F = 375,557$, $df = 1$) with the Mg/Ca ratios increasing with low (26°C) and high (30°C) temperatures after inoculation of the pathogen and the pathogen-with-BMC treatments (Figure 6B).

Specifically, corals inoculated with pathogen at 30°C (treatment P30, 27 mmol/mol ± 4.6 mmol/mol) incorporated more Mg than when only BMC was inoculated (treatment C30, 12.7 mmol/mol ± 2.1 mmol/mol, Tukey's *post-hoc* test, $p < 0.01$), with the highest values observed in corals kept at the treatment PC30 (42.1 mmol/mol ± 10 mmol/mol) in comparison with treatments CTL30 (Tukey's *post-hoc* test, $p < 0.01$), P30 (Tukey's *post-hoc* test, $p < 0.01$), and C30 (Tukey's *post-hoc* test, $p < 0.01$). Despite the presence of the pathogen, the BMC-treated corals showed the lowest Mg/Ca ratios at a temperature of 30°C (treatment C30, 12.7 ± 2.1), leading to rapid calcification at the skeleton surface, while in the BMC treatment alone, the calcification rate was similar to the control samples (Figure 6B). Magnesium is actively transported by the coral skeleton and is strongly regulated by temperature, which in turn affects the calcification rate. Mg seems to affect the formation and calcification of coral skeletons more than Sr (Inoue et al., 2007; Brahmi et al., 2012), being responsible for the formation of biomineral crystals and the shape of skeletal fiber structures. At 30°C, in general, coral begins to undergo bleaching and lose its symbionts. As zooxanthellae provide the necessary energy for calcification and transport of Ca^{2+}, this could be a possible explanation for the low Ca^{2+} absorption at higher temperatures in our experiment (Figure 6B). These values possibly reflect different degrees of adaptation to the mesocosm, specifically to the flux of light and nutrients and the original factors of microhabitats. The branching structure of *P. damicornis* can form microhabitats where one area is better illuminated than another, causing physiological differences, including zooxanthellae population density, which may have provided some factor that initially offered an advantage to some samples. These differences were minimized by the cut done in the coral fragments, lessening the possible microhabitat effect. The similarity between tip × tip demonstrates that the values adjust and come into balance, with only the control remaining different, which maintained the higher Mg/Ca ratios and was close to the initial value (treatment CTL26, 27.8 mmol/mol ± 2.7 mmol/mol). This indicates that the new environment neither helped nor hindered the initial condition of the treatments.

The BMC treatment promoted mitigation of damage observed in the skeleton, especially that caused by *Vibrio* (the pathogen), which closely agrees with the literature evaluating other health proxies (Rosado et al., 2019; Doering et al., 2021; Santoro et al., 2021; Ushijima et al., 2023) and the use of probiotics, and other microbial therapies, as part of a customized medicine approach (Peixoto et al., 2019). Coral calcification was also improved by the BMC consortium under normal conditions (Zhang et al., 2021), although the previous study did not investigate the impact of thermal stress and/or pathogens.

The exposure of the coral to the pathogen with BMCs resulted in a combination of increased porosity, maintenance of SMD, Mg/Ca ratio, and spherulitic crystals, which could be consistent with the thickening of fibers and enhancement of skeletal mechanical properties (Moynihan et al., 2022). However, none of the treatments were able to change the aragonite mineralogy of the coral. This indicates a potentially symbiotic interaction between BMCs and the coral skeleton cells, which should be further investigated. Additional studies will help to elucidate more details regarding the dynamics, location, and physical interactions between pathogens and BMCs with the coral skeleton.

Data availability statement

The original contributions presented in the study are included in the article/Supplementary Material. Further inquiries can be directed to the corresponding author.

Ethics statement

The manuscript presents research on animals that do not require ethical approval for their study.

Author contributions

RP, GD, and CB conceived the experiment(s). RP, MM, CJ, PM, and GD conducted the experiment(s). MM, CB, RP, PM, JT, CS, DF, and GD analyzed the results. CB, RP, DF, AB, and MM wrote the paper. CB, AB, and HE performed the density, MEV, and EDX analyses. DF and HE performed the statistical analyses and DF produced the graphs. JT, MM, and CS performed the micro-CT analysis. All authors contributed to the article and approved the submitted version.

Funding

Acknowledgments

UERJ for the densitometry analysis. Thanks to Rebecca Botticelli for coloring the SEM figures to show the crystal habit. Thanks to Cenpes/Petrobras for the use of the mesocosm structure.

In memoriam

Conflict of interest

Publisher's note

Supplementary material

The Supplementary Material for this article can be found online at: https://www.frontiersin.org/articles/10.3389/fmars.2023.1212690/full#supplementary-material

SUPPLEMENTARY FIGURE 1
Schematic drawing of the mesocosm system used for the experiment: (1) 1.3-L independent experimental aquarium, where the coral fragments were maintained; (2) water bath for maintaining the temperature of the aquariums, cooled with a chiller and heated with heaters and a thermostat; (3) air-injection hoses for oxygenation and water circulation in the independent experimental aquarium; (4) sump, additional plastic container of 25 L in order to increase the volume of water in the aquarium, permanently covered to avoid contamination; (5) centrifugal pump that pumped water from the sump to the aquarium at an adjustable flow rate of 70 L/h, returning from the independent aquarium to the sump by gravity in a closed loop; (6) aquarium overflow connected to the sump by a 0.5-in. (12.7 mm) diameter hose, where the pumped water returned to the sump by gravity; (7) wooden table that supported the entire system. Photograph of mesocosm installed, with MM doing coral husbandry.

SUPPLEMENTARY FIGURE 2
Mean + SD of skeletal structures and chemical changes of the coral *Pocillopora damicornis* in response to pathogen (*Vibrio coralliilyticus*) and probiotic inoculation under ambient conditions (26°C) and thermal stress (30°C). The letters indicate significant ($p < 0.05$) differences among treatments (two-way ANOVA followed by Tukey's *post-hoc* test).

SUPPLEMENTARY TABLE 1
Schematic synthesis of statistical results for Mg/Ca, Sr/Ca, SMC, and SMD based on three-way ANOVA for different temperatures on the skeleton of *Pocillopora damicornis*.

SUPPLEMENTARY TABLE 2
Porosity, median pore-size diameter (MPSD) ($n = 3$), skeletal mineral density (SMD), and skeletal mineral content (SMC) ($n = 1$) of the skeleton surface of *Pocillopora damicornis* under different treatments.

SUPPLEMENTARY TABLE 3
The presence/absence of fiber habit occurrences on the skeleton surface of *Pocillopora damicornis* under different treatments.

SUPPLEMENTARY TABLE 4
Mean values of Sr/Ca and Mg/Ca in µmol/mol from five replicates and Calcium found in the skeleton of *P. damicornis*. Treatments are BMC consortium at 26°C (C26), BMC consortium at 30°C (C30), pathogen *V. coralliilyticus* at 26°C (P26), pathogen *V. coralliilyticus* at 30°C, pathogen and BMC consortium at 26°C (PC26), pathogen and BMC consortium at 30°C (PC30), control at 26°C (CTL26), and control at 30°C (CTL30).

References

Agostini, S., Suzuki, Y., Higuchi, T., Casareto, B. E., Yoshinaga, K., Nakano, Y., et al. (2012). Biological and chemical characteristics of the coral gastric cavity. *Coral Reefs* 31, 147–156. doi: 10.1007/s00338-011-0831-6

Baldock, T. E., Golshani, A., Callaghan, D. P., Saunders, M. I., and Mumby, P. J. (2014). Impact of sea-level rise and coral mortality on the wave dynamics and wave forces on barrier reefs. *Mar. pollut. Bulletin* 83 (1), 155–164. doi: 10.1016/j.marpolbul.2014.03.058

Barker, S., Greaves, M., and Elderfield, H. (2003). A study of cleaning procedures used for foraminiferal Mg/Ca paleothermometry, Geochem. *Geophys. Geosyst.* 4 (9), 8407. doi: 10.1029/2003GC000559

Baums, I. B., Baker, A. C., Davies, S. W., Grottoli, A. G., Kenkel, C. D., Kitchen, S. A., et al. (2019). Considerations for maximizing the adaptive potential of restored coral populations in the western Atlantic. *Ecol. Appl.* 29 (8), e01978. doi: 10.1002/eap.1978

Ben-Haim, Y., Thompson, F. L., Thompson, C. C., Cnockaert, M. C., Hoste, B., Swings, J., et al. (2003). *Vibrio coralliilyticus* sp. nov., a temperature dependent pathogen of the coral *Pocillopora damicornis*. *Int. J. Syst. Evol. Microbiol.* 53, 309–315. doi: 10.1099/ijs.0.02402-0

Bourne, D. G., Morrow, K. M., and Webster, N. S. (2016). Insights into the coral microbiome: underpinning the health and resilience of reef ecosystems. *Annu. Rev. Microbiol.* 70, 317–340. doi: 10.1146/annurev-micro-102215-095440

Brahmi, C., Kopp, C., Domart-Coulon, I., Stolarski, J., and Meibom, A. (2012). Skeletal growth dynamics linked to trace-element composition in the scleractinian coral *Pocillopora damicornis*. Geochim. *Cosmochim. Acta* 99, 146–158. doi: 10.1016/j.gca.2012.09.031

Braz, G. B., Lacerda, C. H. F., Evangelista, H., Güth, A. Z., Rumbelsperger, A. M. B., Capel, K. C. C., et al. (2022). Unprecedented erosion of Mussismilia harttii, a major reef –building species in the southwestern Atlantic, after the 2019 bleaching event. *Coral Reefs* 41, 1537–1548. doi: 10.1007/s00338-022-02303-1

Brindley, G. W., and Brown, G. (1980). *Crystal structures of clay minerals and their X-ray identification* (Monograph 5: Mineralogical Society of Great Britain and Ireland).

Brown, B. E., Hewit, R., and Le Tissier, M. D. (1983). The nature and construction of skeletal spines in *Pocillopora damicornis*. *Coral Reefs* 2, 81–89. doi: 10.1007/BF02395278

Bruno, J. F., Selig, E. R., Casey, K. S., Page, C. A., Willis, B. L., Harvell, C. D., et al. (2007). Thermal stress and coral cover as drivers of coral disease outbreaks. *PloS Biol.* 5 (6), e124. doi: 10.1371/journal.pbio.0050124

Bucher, D. J., Harriott, V. J., and Roberts, L. G. (1998). Skeletal micro-density, bulk density and porosity of acroporid corals. *J. Exp. Mar. Biol. Ecol.* 228, 117–135. doi: 10.1016/S0022-0981(98)00020-3

Cameron, C. M., and Edmunds, P. J. (2014). Effects of simulated fish predation on small colonies of massive Porites spp. and *Pocillopora meandrina*. *Mar. Ecol. Prog. Ser.* 508, 139–148. doi: 10.3354/meps10862

Carpenter, K. E., Abrar, M., Aeby, G., Aronson, R. B., Banks, S., Bruckner, A., et al. (2008). One-third of reef-building corals face elevated extinction risk from climate change and local impacts. *Science* 321 (5888), 560–563. doi: 10.1126/science.1159196

Cervino, J. M., Hayes, R. L., Polson, S. W., Polson, S. C., Goreau, T. J., Martinez, R. J., et al. (2004). Relationship of *Vibrio* species infection and elevated temperatures to

yellow blotch/band disease in Caribbean corals. *Appl. Environ. Microbiol.* 70, 6855–6864. doi: 10.1128/AEM.70.11.6855-6864

Cohen, A., and McConnaughey, T. A. (2003). Geochemical perspective on coral mineralization. *Rev. Min. Geochem.* 54, 151–187. doi: 10.2113/0540151

Cornwall, C. E., Comeau, S., Kornder, N. A., Perry, C. T., Hooidonk, R., DeCarlo, T. M., et al. (2021). Global declines in coral reef calcium carbonate production under ocean acidification and warming. *Proc. Natl. Acad. Sci. U.S.A.* 118, e2015265118. doi: 10.1073/pnas.2015265118

Denis, D. J. (2021). *Univariate, Bivariate, and Multivariate Statistics Using R: Quantitative Tools for Data Analysis and Data Science* (New Jersey, USA: John Wiley & Sons), 373.

Doering, T., Wall, M., Putchim, L., Rattanawongwan, T., Schroeder, R., Hentschel, U., et al. (2021). Towards enhancing coral heat tolerance: a "microbiome transplantation" treatment using inoculations homogenized coral tissues. *Microbiome* 9, 102. doi: 10.1186/s40168-021-01053-6

D'Olivo, J. P., and McCulloch, M. T. (2017). Response of coral calcification and calcifying fluid composition to thermally induced bleaching stress. *Sci. Rep.* 7, 2207. doi: 10.1038/s41598-017-02306-x

Domart-Coulon, I., Tambutté, S., Tambutté, E., and Allemand, D. (2004). Short term viability of soft tissue detached from the skeleton of reef-building corals. *J. Exp. Mar. Biol. Ecol.* 309, 199–217. doi: 10.1016/j.jembe.2004.03.021

Dove, S. G., Takabayashi, M., and Hoegh-Guldberg, O. (1995). Isolation and partial characterization of the pink and blue pigments of Pocilloporid and Acroporid corals. *Biol. Bull.* 189, 288–297. doi: 10.2307/1542146

Dunn, J. G., Sammarco, P. W., and LaFleur, G. Jr. (2012). Effects of phosphate on growth and skeletal density in the scleractinian coral *Acropora muricata*: A controlled experimental approach. *J. Exp. Mar. Biol. Ecol.* 411, 34–44. doi: 10.1016/j.jembe.2011.10.013

Fantazzini, P., Mengoli, S., Pasquini, L., Bortolotti, V., Brizi, L., Mariani, M., et al. (2015). Gains and losses of coral skeletal porosity changes with ocean acidification acclimation. *Nat. Commun.* 6, 7785. doi: 10.1038/ncomms8785

Foster, T., Falter, J. L., McCulloch, M. T., and Clode, P. L. (2016). Ocean acidification causes structural deformities in juvenile coral skeletons. *Sci. Adv.* 2, e1501130. doi: 10.1126/sciadv.1501130

Fragoso dos Santos, H., Duarte, G. A. S., Rachid, C. T. C. C., Chaloub, R. M., Calderon, E. N., Marangoni, L. F. B., et al. (2015). Impact of oil spills on coral reefs can be reduced by bioremediation using probiotic microbiota. *Sci. Rep.* 5, 18268. doi: 10.1038/srep18268

Hair, J. F., Anderson, R. E., Babin, B. J., and Black, W. C. (2010). *Multivariate data analysis: A global perspective (Vol. 7)* (Englewood Cliffs, NJ: Prentice Hall), 761.

Herndl, G. J., and Velimirov, B. (1985). Bacteria in the coelenteron of Anthozoa: control of coelomic bacterial density by the coelenteric fluid. *J. Exp. Mar. Biol. Ecol.* 93, 115–130. doi: 10.1016/0022-0981(85)90153-4

Hetzinger, S., Pfeiffer, M., Dullo, W.-C., Zinke, J., and Garbe-Schönberg, D. (2016). A change in coral extension rates and stable isotopes after El Niño-induced coral bleaching and regional stress events. *Sci. Rep.* 6, 32879. doi: 10.1038/srep32879

Hofmann, L. C., Straub, S., and Bischof, K. (2013). Elevated CO_2 levels affect the activity of nitrate reductase and carbonic anhydrase in the calcifying rhodophyte *Corallina officinalis*. J. Exp. Bot. 64, 899–908. doi: 10.1093/jxb/ers369

Horvath, K. M., Castillo, K. D., Armstrong, P., Westfield, I. T., Courtney, T., and Ries, J. B. (2016). Next-century Ocean acidification and warming both reduce calcification rate, but only acidification alters skeletal morphology of reef-building coral *Siderastrea siderea*. Sci. Rep. 6, 29613. doi: 10.1038/srep29613

Howe, S. A., and Marshall, A. T. (2002). Temperature effects on calcification rate and skeletal deposition in the temperate coral, *Plesiastrea versipora* (Lamarck). *J. Exp. Mar. Biol. Ecol.* 275, 63–81. doi: 10.1016/S0022-0981(02)00213-7

Inoue, M., Suzuki, A., Nohara, M., Hibino, K., and Kawahata, H. (2007). Empirical assessment of coral Sr/Ca and Mg/Ca ratios as climate proxies using colonies grown at different temperatures, Geophys. Res. Lett. 34, L12611. doi: 10.1029/2007GL029628

Isa, Y. (1986). An electron microscope study on the mineralization of the skeleton of the staghorn coral *Acropora hebes*. Mar. Biol. 93, 91–101. doi: 10.1007/BF00428658

Knowlton, N., Grottoli, AG., Kleypas, J., Obura, D., Corcoran, E., de Goeij, JM., et al (2021). *Rebuilding coral reefs: A decadal grand challenge* (International Coral Reef Society and Future Earth Coasts), 56. doi: 10.53642/NRKY9386

Koop, K., Booth, D., Broadbent, A., Brodie, J., Bucher, D., Capone, D., et al. (2001). ENCORE: the effect of nutrient enrichment on coral reefs. Synthesis of results and conclusions. *Mar. Poll. Bull.* 42, 91–120. doi: 10.1016/s0025-326x(00)00181-8

Kooperman, N., Ben-Dov, E., Kramarsky-Winter, E., Barak, Z., and Kushmaro, A. (2007). Coral mucus-associated bacterial communities from natural and aquarium environments. *FEMS Microbiol. Lett.* 276, 106–113. doi: 10.1111/j.1574-6968.2007.00921.x

Koren, O., and Rosenberg, E. (2006). Bacteria associated with mucus and tissues of the coral *Oculina patagonica* in summer and winter. *Appl. Environ. Microbiol.* 72, 5254–5259. doi: 10.1128/AEM.00554-06

Lesser, M. P., Mazel, C. H., Gorbunov, M. Y., and Falkowski, P. G. (2004). Discovery of symbiotic nitrogen fixing cyanobacteria in corals. *Science* 305, 997–1000. doi: 10.1126/science.1099128

Linnaeus, C. (1758). Systema naturæ per Regna tria naturæ, secundum classes, ordines, genera, species, cum characteribus, differentiis, synonymis, locis. *Tomus I. Editio decima, reformata. Holmiæ, Laurentii Salvii, [iv] + 824* doi: 10.5962/bhl.title.542

Marshall, A. T., and Clode, P. (2004). Effects of calcium-free and low-calcium artificial seawater on polyps of a scleractinian coral *Galaxea fascicularis*. Coral Reefs 23, 277–280. doi: 10.1007/s00338-004-0371-4

Mass, T., Giuffre, A. J., Sun, C. Y., Stifler, C. A., Frazier, M. J., Neder, M., et al. (2017). Amorphous calcium carbonate particles form coral skeletons. *Proc. Natl. Acad. Sci. U.S.A.* 114, E7670–E7678. doi: 10.1073/pnas.1707890114

Meibom, A., Cuif, J.-P., Hillion, F., Constantz, B. R., Juillet-Leclerc, A., Dauphin, Y., et al. (2004). Distribution of magnesium in coral skeleton. *Geophys. Res. Lett.* 31, L23306. doi: 10.1029/2004GL021313

Milliman, J. D. (1993). Production and accumulation of calcium carbonate in the ocean: Budget of a non-steady state. *Global Biogeochem. Cycles* 7, 927–957. doi: 10.1029/93GB02524

Mollica, N. R., Guo, W., Cohen, A. L., Huang, K. F., Foster, G. L., Donald, H. K., et al. (2018). Ocean acidification affects coral growth by reducing skeletal density. *Proc. Natl. Acad. Sci. U.S.A.* 115 (8), 1754–1759. doi: 10.1073/pnas.1712806115

Morgans, C. A., Hung, J. Y., Bourne, D. G., and Quigley, K. M. (2020). Symbiodiniaceae probiotics for use in bleaching recovery. *Restor. Ecol.* 28, 282–288. doi: 10.1111/rec.13069

Moynihan, M. A., Amini, S., Oalmann, J., Chua, J. I., Tanzil, J. T., Fan, T. Y., et al. (2022). Crystal orientation mapping and microindentation reveal anisotropy in *Porites* skeletons. *Acta Biomater.* 151, 446–456. doi: 10.1016/j.actbio.2022.08.012

Mwachireya, S. A., McClanahan, T. R., Cote, I. M., and Hartwick, B. E. (2016). Increased terrestrial perturbations modify skeletal properties and mechanical strength of hard corals. *Environ. Nat. Resour. Res.* 6 (4), 153–173. doi: 10.5539/enrr.v6n4p153

Nothdurft, L. D., and Webb, G. E. (2007). Microstructure of common reef-building coral genera *Acropora*, *Pocillopora*, *Goniastrea* and *Porites*: constraints on spatial resolution in geochemical sampling. *Facies* 53, 1–26. doi: 10.1007/s10347-006-0090-0

Peixoto, R. S., Rosado, P. M., Leite, D. C. D. A., Rosado, A. S., and Bourne, D. G. (2017). Beneficial Microorganisms for Corals (BMC): proposed mechanisms for coral health and resilience. *Front. Microbiol.* 8. doi: 10.3389/fmicb.2017.00341

Peixoto, R. S., Sweet, M., and Bourne, D. (2019). Customized medicine for corals. *Front. Mar. Sci.* 6. doi: 10.3389/fmars.2019.00686

Peixoto, R. S., Sweet, M., Villela, H. D., Cardoso, P., Thomas, T., Voolstra, C. R., et al. (2021). Coral probiotics: premise, promise, prospects. *Annu. Rev. Anim. Biosci.* 9, 265–288. doi: 10.1146/annurev-animal-090120-115444

Peixoto, R. S., and Voolstra, C. R. (2023). The baseline is already shifted: marine microbiome restoration and rehabilitation as essential tools to mitigate ecosystem decline. *Front. Mar. Sci.* 10. doi: 10.3389/fmars.2023.1218531

Peixoto, R. S., Voolstra, C. R., Sweet, M., Duarte, CD., Carvalho, S., Villela, H., et al. (2022). Harnessing the microbiome to prevent global biodiversity loss. *Nat. Microbiol.* 7, 1726–1735. doi: 10.1038/s41564-022-01173-1

Pernice, M., Raina, J. B., Rädecker, N., Cárdenas, A., Pogoreutz, C., and Voolstra, C. R. (2020). Down to the bone: the role of overlooked endolithic microbiomes in reef coral health. *ISME J.* 14, 325–334. doi: 10.1038/s41396-019-0548-z

Pisapia, C., and Pratchett, M. S. (2014). Spatial variation in background mortality among dominant coral taxa on Australia's Great Barrier Reef. *PloS One* 9 (6), e100969. doi: 10.1371/journal.pone.0100969

Pollock, F. J., McMinds, R., Smith, S., Bourne, D. G., Willis, B. L., Medina, M., et al. (2018). Coral-associated bacteria demonstrate phylosymbiosis and cophylogeny. *Nat. Commun.* 9, 4921. doi: 10.1038/s41467-018-07275-x

Ralph, P. J., Schreiber, U., Gademann, R., Kühl, M., and Larkum, A. W. (2005). Coral photobiology studied with a new imaging pulse amplitude modulated fluorometer. *J. Phycol.* 41, 335–342. doi: 10.1111/j.1529-8817.2005.04034.x

R Core Team (2020) *R: A Language and Environment for Statistical Computing*. Available at: https://www.r-project.org/.

Reshef, L., Koren, O., Loya, Y., Zilber-Rosenberg, I., and Rosenberg, E. (2006). The coral probiotic hypothesis. *Environ. Microbiol.* 8, 2068–2073. doi: 10.1111/j.1462-2920.2006.01148.x

Reynaud, S., Leclercq, N., Romaine-Lioud, S., Ferrier-Pagés, C., Jaubert, J., and Gattuso, J. P. (2003). Interacting effects of CO_2 partial pressure and temperature on photosynthesis and calcification in a scleractinian coral. *Global Change Biol.* 9, 1660–1668. doi: 10.1046/j.1365-2486.2003.00678.x

Ricci, F., Rossetto Marcelino, V., Blackall, L. L., Kühl, M., Medina, M., and Verbruggen, H. (2019). Beneath the surface: community assembly and functions of the coral skeleton microbiome. *Microbiome* 7, 159. doi: 10.1186/s40168-019-0762-y

Ritchie, K. B. (2006). Regulation of microbial populations by coral surface mucus and mucus-associated bacteria. *Mar. Ecol. Prog. Ser.* 322, 1–14. doi: 10.3354/meps322001

Roche, R. C., Abel, R. L., Johnson, K. G., and Perry, C. T. (2011). Spatial variation in porosity and skeletal element characteristics in apical tips of the branching coral *Acropora pulchra* (Brook 1891). *Coral Reefs* 30, 195–201. doi: 10.1007/s00338-010-0679-1

Rodriguez-Lanetty, M., Harii, S., and Hoegh-Guldberg, O. (2009). Early molecular responses of coral larvae to hyperthermal stress. *Mol. Ecol.* 18, 5101–5114. doi: 10.1111/j.1365-294X.2009.04419.x

Rohwer, F., Seguritan, V., Azam, F., and Knowlton, N. (2002). Diversity and distribution of coral-associated bacteria. *Mar. Ecol. Prog. Ser.* 243, 1–10. doi: 10.3354/meps243001

Rollion-Bard, C., and Blamart, D. (2015). Possible controls on Li, Na, and Mg incorporation into aragonite coral skeletons. *Chem. Geol.* 396, 98–111. doi: 10.1016/j.chemgeo.2014.12.011

Rosado, P. M., Leite, D. C., Duarte, G. A., Chaloub, R. M., Jospin, G., Nunes da Rocha, U., et al. (2019). Marine probiotics: increasing coral resistance to bleaching through microbiome manipulation. *ISME J.* 13, 921–936. doi: 10.1038/s41396-018-0323-6

Santoro, E. P., Borges, R. M., Espinoza, J. L., Freire, M., Messias, C. S. M. A., Villela, H. D. M., et al. (2021). Coral microbiome manipulation elicits metabolic and genetic restructuring to mitigate heat stress and evade mortality. *Sci. Adv.* 7, eabg3088. doi: 10.1126/sciadv.abg3088

Shirai, K., Kawashima, T., Sowa, K., Watanabe, T., Nakamori, T., Takahata, N., et al. (2008). Minor and trace element incorporation into branching coral *Acropora nobilis* skeleton. *Geochim. Cosmochim. Acta* 72, 5386–5400. doi: 10.1016/j.gca.2008.07.026

Siebeck, U. E., Marshall, N. J., Klüter, A., and Hoegh-Guldberg, O. (2006). Monitoring coral bleaching using a color reference card. *Coral Reefs* 25, 453–460. doi: 10.1007/s00338-006-0123-8

Silva, D. P., Duarte, G., Villela, H. D., Santos, H. F., Rosado, P. M., Rosado, J. G., et al. (2019). Adaptable mesocosm facility to study oil spill impacts on corals. *Ecol. Evol.* 9, 5172–5185. doi: 10.1002/ece3.5095

Sinclair, D. J. (2005). Correlated trace element 'vital effects' in tropical corals: A new tool for probing biomineralization chemistry. *Geochim. Cosmochim. Acta* 69, 3265–3284. doi: 10.1016/j.gca.2005.02.030

Spiske, M., Böröcz, Z., and Bahlburg, H. (2008). The role of porosity in discriminating between tsunami and hurricane emplacement of boulders — A case study from the Lesser Antilles, southern Caribbean. *Earth Planet. Sci. Lett.* 268, 384–396. doi: 10.1016/j.epsl.2008.01.030

Stolarski, J. (2003). *Three-dimensional micro and nanostructural characteristics of the scleractinian coral skeleton: A biocalcification proxy* Vol. 48 (Warszawa, Poland: Acta Palaeontol. Pol), 497–530. Available at: https://www.app.pan.pl/archive/published/app48/app48-497.pdf.

Sun, C.-Y. (2017). Spherulitic growth of coral skeletons and synthetic aragonite: Nature's three-dimensional printing. *ACS Nano* 11, 6612–6622. doi: 10.1021/acsnano.7b00127

Takabayashi, M. (1996). Impacts of in *situ* inorganic nutrient enrichment on the scleractinian corals, *Stylophora pistillata* and *Pocillopora damicornis* (Australia: University of Sydney).

Ushijima, B., Gunasekera, S. P., Meyer, J. L., Tittl, J., Pitts, KA., Thompson, S., et al. (2023). Chemical and genomic characterization of a potential probiotic treatment for stony coral tissue loss disease. *Commun. Biol.* 6, 248. doi: 10.1038/s42003-023-04590-y

Vezzulli, L., Previati, M., Pruzzo, C., Marchese, A., Bourne, D. G., Cerrano, C., et al. (2010). Vibrio infections triggering mass mortality events in a warming Mediterranean Sea. *Environ. Microbiol.* 12, 2007–2019. doi: 10.1111/j.1462-2920.2010.02209.x

Voolstra, C. R., Suggett, D. J., Peixoto, R. S., Parkinson, J. E., Quigley, K. M., Silveira, C. B., et al. (2021). Extending the natural adaptive capacity of coral holobionts. *Nat. Rev. Earth Environ.* 2, 747–762. doi: 10.1038/s43017-021-00214-3

Voolstra, C. R., and Ziegler, M. (2020). Adapting with microbial help: microbiome flexibility facilitates rapid responses to environmental change. *BioEssays* 42, e2000004. doi: 10.1002/bies.202000004

Walsh, S., Brading, P., Suggett, D. J., and Smith, D. J. (2012). "Working with nature to identify coral reefs with increased environmental tolerance," in *Proc. of the 12th Int. Coral Reef Symp*, Cairns, Australia, 9-13 July, Coral bleaching and climate change. (Cairns, Australia: ICRS - International Coral Reef Society).

Ward, J. R., Kim, K., and Harvell, C. D. (2007). Temperature affects coral disease resistance and pathogen growth. *Mar. Ecol. Prog. Ser.* 329, 115–121. doi: 10.3354/meps329115

Welsh, R. M., Rosales, S. M., Zaneveld, J. R., Payet, J. P., McMinds, R., Hubbs, S. L., et al. (2017). Alien vs. predator: bacterial challenge alters coral microbiomes unless controlled by *Halobacteriovorax* predators. *PeerJ* 5, e3315. doi: 10.7717/peerj.3315

Yang, S.-H., Lee, S. T., Huang, C. R., Tseng, C. H., Chiang, P. W., Chen, C. P., et al. (2016). Prevalence of potential nitrogen-fixing, green sulphur bacteria in the skeleton of reef-building coral *Isopora palifera*. *Limnol. Oceanogr.* 61, 1078. doi: 10.1002/lno.10277

Zhang, Y., Yang, Q., Ling, J., Long, L., Huang, H., Yin, J., et al. (2021). Shifting the microbiome of a coral holobiont and improving host physiology by inoculation with a potentially beneficial bacterial consortium. *BMC Microbiol.* 21, 130. doi: 10.1186/s12866-021-02167-5

Zhou, Y., Tang, K., Wang, P., Wang, W., Wang, Y., and Wang, X. (2020). Identification of bacteria-derived urease in the coral gastric cavity. *China Earth Sci.* 63, 1553–1563. doi: 10.1007/s11430-020-9647-x